

# FLUID DYNAMICS AND SOLIDIFICATION OF MOLTEN SOLDER DROPLETS IMPACTING ON A SUBSTRATE IN MICROGRAVITY

C. M. Megaridis<sup>1</sup>, D. Poulikakos<sup>2</sup>, G. Diversiev<sup>1</sup>, K. Boomsma<sup>1</sup>, B. Xiong<sup>1</sup> and V. Nayagam<sup>3</sup>, <sup>1</sup>Department of Mechanical Engineering, University of Illinois at Chicago, Chicago IL 60607-7022, cmm@uic.edu, <sup>2</sup>Institute of Energy Technology, Swiss Federal Institute of Technology, ETH Center, CH-8092 Zurich, Switzerland, <sup>3</sup>National Center for Microgravity Research, Cleveland, Ohio 44135.

## INTRODUCTION

This program investigates the fluid dynamics and simultaneous solidification of molten solder droplets impacting on a flat substrate. The problem of interest is directly relevant to the printing of microscopic solder droplets in surface mounting of microelectronic devices. The study consists of a theoretical and an experimental component. The theoretical work uses axisymmetric Navier-Stokes models based on finite element techniques. The experimental work will be ultimately performed in microgravity in order to allow for the use of larger solder droplets which make feasible the performance of accurate measurements, while maintaining similitude of the relevant fluid dynamics groups (Re, We).

A schematic of the two distinct stages (flight and impact) of the problem examined is shown in Fig. 1. The primary application of interest (solder microdroplet dispensing) employs solder droplets approximately 50 to 100  $\mu\text{m}$  in diameter, which collide, spread, recoil and eventually solidify on the substrate. Due to the small size of the droplets and the relatively high surface tension coefficient of solder, gravity effects are negligible. This solder application technology has shown great promise in microelectronic packaging and assembly, therefore, the development of a good understanding of the pertinent fluid dynamics and solidification phenomena is essential for its successful commercial implementation. However, progress in this area has been hindered by the small length scales of the problem (50 to 100  $\mu\text{m}$ ), which have made experimental measurements of the relevant transport phenomena difficult. Alternative approaches, which employed much larger (mm-size) droplets, yielded results that were affected by the masking effects of gravity. Hence, even though mm-size droplets yield significantly improved resolution, the applicability of the obtained results for much smaller droplets remains suspect. Conducting experiments in a microgravity environment eliminates the unwanted influence of gravity and makes the ex-

perimental investigation of large droplet dispersion directly relevant.

The Reynolds, Weber and Froude numbers characteristic of the process shown in Fig. 1 are defined by

$$\text{Re} = \frac{V_0 d_0}{\nu}, \quad \text{We} = \frac{\rho V_0^2 d_0}{\gamma}, \quad \text{Fr} = \frac{V_0^2}{d_0 g} \quad (1)$$

where  $V_0$ ,  $d_0$  denote droplet impact velocity and diameter, while  $\rho$ ,  $\nu$ ,  $\gamma$  correspond to the density, kinematic viscosity and surface tension coefficient of the liquid. To exemplify the disparity in the importance of gravity in the dispersion of large and small droplets, the values of Re, We and Fr were calculated for a set of parameters corresponding to the real dispersion process in normal gravity (50 micron diameter solder droplet impacting on a flat surface with a velocity 1m/s). These values were Re=157, We=1.2, Fr=2038, and illustrate the importance of inertia and surface tension, as well as the insignificance of gravity effects. If a larger (1mm) drop is used in normal gravity experiments, a slower impact velocity  $V_0$  is required for similitude based on Re. In turn, similitude in terms of the Weber number requires a smaller surface tension coefficient. To maintain similitude in this specific example, the surface tension coefficient as well as the impact velocity of the larger droplets need be reduced by twenty-fold. The resulting values of the above dimensionless groups are then Re=157, We=1.2 and Fr=0.25. Clearly, the drastic decrease in the value of the Froude number proves that gravity effects become significant for mm-size droplets, and that the presence of a microgravity environment is necessary in large solder-droplet impact experiments.

## OBJECTIVE

The study aims to create a science base and identify the influence of the dominant process parameters in solder droplet dispensing. These parameters are: droplet size and velocity; droplet, substrate and ambient gas temperatures; and contact angle between solder and substrate before and after solidification. The sensitivity of the solidified-droplet (bump) shape and

size to variations in the above parameters is critical because solder bump volume, position, and height variation are key metrics for solder jet technology. Through a combination of experiments and numerical modeling, the effect of the dimensionless groups defined in Eq. (1) and the physics they represent are systematically documented.

## METHODOLOGY

The research consists of a theoretical and an experimental component. The theoretical component investigates the fluid dynamics and solidification of a molten solder droplet during its impact on the substrate, in order to attain a fundamental understanding of the miniature solder deposition process. The experimental component tests the numerical predictions and provides necessary input data (such as wetting angles) for the theoretical model. Details of both components are given below.

### Theoretical

The model simulates the axisymmetric impact and subsequent solidification of an initially spherical, molten solder droplet on a flat multi-layer composite substrate. When a gravitational field is present, the droplet is injected along that direction, which is orthogonal to the target surface. The Navier-Stokes equations combined with heat transfer and solidification are solved in the liquid phase using a Lagrangian approach. The heat conduction equation is solved in the solid phase, i.e., substrate and solidified sector of the droplet. It is noted that the employed axisymmetric approach is valid for situations where the solder droplet impinges on the substrate at an angle equal or approaching 90°. The mathematical model formulation has been described elsewhere in detail (see Waldvogel et al., 1996; Waldvogel and Poulidakos, 1997) and will not be repeated here for brevity. However, a brief description is given in the following for completeness.

**Fluid Dynamics:** Laminar flow of a constant property fluid (molten solder) is assumed. The radial and axial components of the momentum equation are considered along with the continuity equation. The artificial compressibility method is employed, thus introducing a pressure term to the mass conservation equation. The free surface deformation is tracked by the two corresponding stress balance equations (along  $r$  and  $z$ ). The wetting force at the dynamic contact line between the liquid droplet and the substrate is neglected

throughout the analysis. This assumption is valid during the initial stages of droplet impact where inertia forces are high with respect to the retarding forces of viscosity and surface tension. In the case of solder jetting, solidification occurs very quickly at the contact area, thus eliminating the need for a wetting condition altogether. The moving contact line is treated by allowing for slipping along the radial direction (Dussan, 1979).

**Heat Transfer:** The Lagrangian formulation is used for the conjugate heat transfer process in the droplet and the substrate. The energy conservation equation is solved in the droplet interior as well as in the substrate. Heat transfer from all exposed surfaces is neglected.

**Thermal Contact Resistance:** Thermal contact resistance between droplet and substrate is modeled by a thin layer of arbitrary thickness. This layer is assigned zero heat capacity and experiences only axial conduction. Thermal contact resistance is quantified by a dimensionless coefficient (Biot number), defined by

$$Bi = \frac{h_c d_0}{k_0} \quad (2)$$

where  $h_c$  denotes the heat transfer coefficient for the thin contact area between the droplet and the substrate,  $k_0$  the thermal conductivity of the solder and  $d_0$  the droplet diameter before impact. Unfortunately, no correlations published to date have been identified to determine the value of  $h_c$  in the parametric domain of solder jetting. To this end, specific attention is given to identify the thermal contact resistance in solder microdroplet dispensing and, in turn, facilitate future studies in this area.

**Solidification:** The following assumptions are made regarding the solidification of the molten-solder droplet. First, since a eutectic alloy is studied, a sharp boundary separating distinct liquid and solid regions is included in the model. Furthermore, it is assumed that phase change occurs at the equilibrium freezing temperature (i.e., no undercooling is considered). It is noted that the droplet solid and liquid phase densities are nearly identical since the 63% Sn–37% Pb solder material experiences only a 0.2% contraction upon freezing. The exact specific heat method proposed by Bushko and Grosse (1991) was adopted to model solidification. This approach facilitates the finite element formulation and has the added advantage that it is very accurate in conserving energy as the droplet solidifies.

## Numerical Solution Procedure

The computational domain is discretized with a mesh of triangular elements, and the numerical model is solved using a Galerkin finite element method. Quadratic and linear shape functions are used for velocity and pressure, respectively. An implicit method is utilized for the numerical integration of the fluid dynamics equations in time, while a Crank-Nicholson scheme is used for the energy equation. The details of the iterative solution technique and mesh generation algorithm are given in Waldvogel and Poulikakos (1997). The spatial resolution needed to provide grid and time-step independence is  $\sim 600$  nodes in the droplet and  $\sim 1,100$  nodes in the substrate. A dimensionless time step of  $\delta t V_0/d_0 = 5 \times 10^{-4}$  was found adequate for time-step insensitive results.

## Experimental

Two separate jetting apparatus are employed in the experiments. The first is capable of jetting 50-80 $\mu\text{m}$  solder droplets with velocities  $\sim 1\text{m/s}$ , while the other generates mm-sized droplets at injection speeds of  $\sim 0.1\text{m/s}$ . Both devices create droplets on demand, and feature heated reservoirs, in which high-purity 63%Sn-37%Pb solder is maintained at temperatures  $\sim 210^\circ\text{C}$  (melting point of solder is  $183^\circ\text{C}$ ). The first device uses nitrogen gas to pressurize the system forming the droplets, thus hindering the formation of oxides within the reservoir. Individual droplets are generated as a voltage pulse excites a piezoelectric transducer mounted within the device. The second device (which forms larger droplets) utilizes mechanical forcing of the solder pool (via a plunger) through a round orifice at the bottom of the reservoir. The droplet flight occurs in a nitrogen atmosphere to avoid oxygen adsorption on the solder surface. The presence of oxygen is avoided because it is known to degrade the surface properties of liquid solder. The impact velocity  $V_0$  of the small droplets is determined using a stroboscope and a steady stream of droplets generated at a known injection frequency. For the larger droplets, a high-speed video system is used to measure droplet impact velocities.

The solidified shape of the small deposited droplets is evaluated using scanning electron microscopy (SEM). The experimental results reported in the following section were all obtained in normal gravity. Small droplets impacted on a two-layer composite substrate (Ni on Si). For the larger (mm) droplets, the substrates consisted of a single-layer metal material.

## RESULTS AND DISCUSSION

### Thermal Contact Resistance of Microdroplets

The thermal contact resistance between a typical electronic substrate and impacting solder droplets was examined first. The chosen conditions correspond to a 63%Sn-37%Pb solder droplet with pre-impact diameter  $d_0=53\mu\text{m}$ , velocity  $V_0=1.6\text{m/s}$  and temperature  $210^\circ\text{C}$ . The two-layered substrate (consisting of a  $2\mu\text{m}$ -thick nickel layer on a  $212\mu\text{m}$  layer of silicon) had an initial temperature of  $35^\circ\text{C}$ . The dimensionless numbers corresponding to these baseline conditions are  $\text{Re}=266$ ,  $\text{We}=3.23$  and  $\text{Fr}=4930$ . These operating conditions are characteristic of practical situations, and have been chosen primarily because of the availability of experimental data; see Waldvogel and Poulikakos (1997), as well as Xiong et al. (1998).

A series of model simulations was performed with all process parameters fixed to the baseline values stated above, while the values of  $Bi$  were varied over a range from 0.01 to 0.75. These values of  $Bi$  correspond to contact heat transfer coefficients  $h_c$  in the range 4-350  $\text{kW/m}^2\text{K}$ . Even though the value of  $Bi$  changed from run to run, it was kept constant throughout each of these simulations. The computed solder bump outline for each value of  $Bi$  revealed that this shape is very sensitive to the contact resistance between droplet and substrate; see Xiong et al. (1998). Figure 2 presents two geometric parameters describing the solidified-bump shape and its dependence on thermal contact resistance. Both parameters are plotted in their dimensionless form versus Biot number (likewise, heat transfer coefficient  $h_c$ ). Two values of height ( $z/d_0$ ) for each solidified bump appear in Fig. 2: one on the symmetry axis and another at the off-axis location of maximum elevation. It is clear that for all values of  $Bi$  examined, these two heights are essentially identical. Figure 2 also shows that the predicted bump height varies by up to 20% depending on thermal contact resistance; the maximum height is realized at  $Bi=0.1$  (or  $h_c=47.2\text{kW/m}^2\text{K}$ ). These variations of bump dimensions with thermal contact resistance can be critical in solder jetting, as solder bump height deviations of only a few percent can be detrimental to the successful implementation of the technique in high-precision electronic component manufacturing. The dimensionless contact area  $(d_{con}/d_0)^2$  between the solidified solder droplet and the substrate is also shown in Fig. 2 and demonstrates a weaker dependence on thermal contact resistance, with an overall increasing trend towards higher values of  $Bi$  or  $h_c$ .

According to this trend, more efficient heat transport results in larger contact area, and, in turn, better attachment of the bump on the substrate.

A detailed comparison of several computed bump shapes with those determined experimentally was conducted, see Xiong et al. (1998), to determine the value(s) of  $Bi$  which provided the best match between the two shapes. Shape comparisons were conducted by means of the morphology of the ripples on the outline of the bump (see Fig. 3), and by measuring the contact area at the bump base. A phase-dependent value of  $Bi$  allowed best agreement between experiment and modeling. More specifically, the value  $Bi_l=0.5$  ( $h_c=235$  kW/m<sup>2</sup> K) was identified for liquid solder/substrate contact, and the value  $Bi_s=0.0275$  ( $h_c=13$  kW/m<sup>2</sup> K) for solid solder/substrate contact. Figure 3a shows the bump geometry obtained in the experiments under the baseline conditions. Figure 3b displays the respective model-predicted shape when the above-mentioned values of  $Bi_l$  and  $Bi_s$  were used. It was concluded that the best agreement between experiment and modeling occurs when the thermal contact between solder and the substrate is reduced nearly by twenty-fold with the appearance of the solid phase.

### Impact of Large Droplets

The results presented in this section were obtained in normal gravity and are discussed to demonstrate the capabilities of the solder-droplet generation apparatus and the high-speed visualization equipment. Both will be implemented in the pending microgravity experiments which will involve mm-sized droplets.

A 63%Sn–37%Pb solder droplet with pre-impact diameter  $d_0=0.9$ mm, velocity  $V_0=0.6$ m/s and temperature 210°C was visualized using high-speed video during its collision with a smooth stainless steel substrate at a temperature of 20°C. The dimensionless numbers corresponding to these conditions are  $Re=1676$ ,  $We=7.4$  and  $Fr=37$ . Figure 4 presents the temporal variation of two geometric parameters describing instantaneous droplet shape from impact up to complete solidification. These parameters are maximum height  $z_{max}$  and maximum splat diameter  $d_{max}$ , both of which change during the dynamic stages of the impact event. Both maximum height and diameter have been normalized in Fig. 4 with respect to  $d_0$ ; time is also presented in a dimensionless form, i.e.,  $t^*=tV_0/d_0$ . The oscillatory nature of the event is apparent in both curves of Fig. 4. The error bars drawn over selected points of the curves shown in Fig. 4a and 4b indicate the uncertainty tied to pixel size resolution. It

is noted that time zero in Fig. 4 corresponds to the first acquired image where contact of the droplet and substrate was visualized. In this case, time zero does not correspond to the instant when contact between the two bodies was first established (time resolution is 1ms). The shape of the solidified bump is shown by the inset of Fig. 4b.

Figure 5 presents selected experimental images obtained via high-speed video when a 0.9mm solder droplet impacted on a smooth copper substrate of temperature 25°C. The initial droplet temperature was 210°C, and the impact velocity was 1.14m/s. The non-dimensional numbers corresponding to these conditions are  $Re=3200$ ,  $We=27.7$  and  $Fr=147.5$ . In the shown sequence, time proceeds from left to right and from top to bottom. Under the above conditions, breakup of the droplet was revealed at the end of the first recoiling cycle after impact. The smaller droplet created by this breakup was subsequently reattached to the main mass, eventually creating a solid bump showing no apparent signs of the earlier separation event (see bottom right frame).

### Acknowledgment

This work was supported by NASA Grant NAG3-1905.

### REFERENCES

- Bushko, W. and Grosse, I. R., 1991, "New Finite Element Method for Multidimensional Phase Change Heat Transfer Problems," *Num. Heat Transfer, Part B*, Vol. 19, pp. 31-48.
- Dussan V., E. B., 1979, "On the Spreading of Liquids on Solid Surfaces: Static and Dynamic Contact Lines," *Ann. Rev. Fluid Mech.*, Vol. 11, pp. 371-400.
- Waldvogel, J. M., Poulidakos, D., Wallace, D. B., and Marusak, R., 1996, "Transport Phenomena in Picoliter Size Solder Droplet Dispersion," *Transactions of the ASME, J. Heat Transfer*, Vol. 118, pp. 148-156.
- Waldvogel, J. M. and Poulidakos, D., 1997, "Solidification Phenomena in Picoliter Size Solder Droplet Deposition on a Composite Substrate," *Int. J. Heat Mass Transfer*, Vol. 40, pp. 295-309.
- Xiong, B., Megaridis, C. M., Poulidakos, D. and Hoang, H., 1998, "An Investigation of Key Factors Affecting Solder Microdroplet Deposition," *ASME, J. Heat Transfer*, Vol. 120, pp. 259-270.

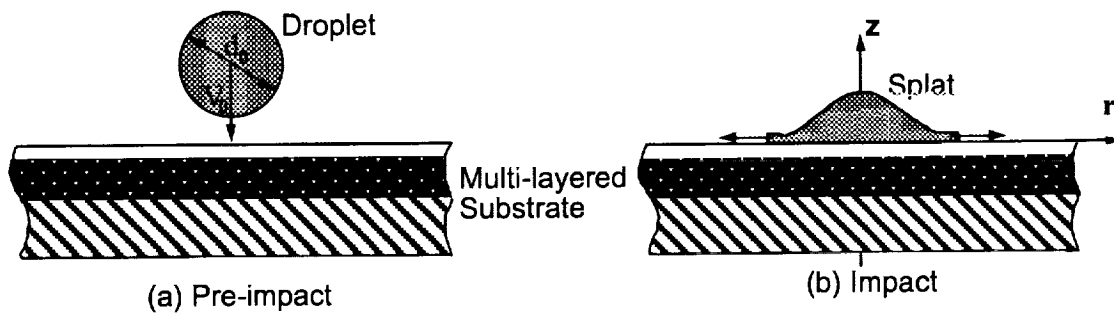


Fig. 1 Basic stages in solder microdroplet dispensing: (a) Flight, (b) Impact.

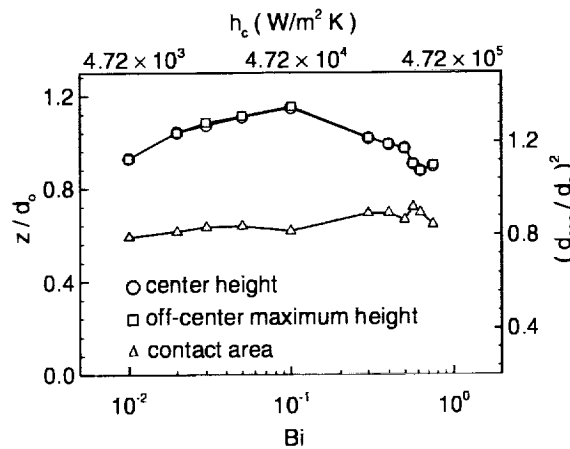


Fig. 2 Geometric parameters describing the solder bump shape and its dependence on thermal contact resistance:  $z/d_0$  denotes the dimensionless height either on the symmetry axis (circles) or at the off-axis location of maximum elevation (squares);  $(d_{con}/d_0)^2$  denotes the dimensionless contact area between the solidified solder droplet and the substrate.

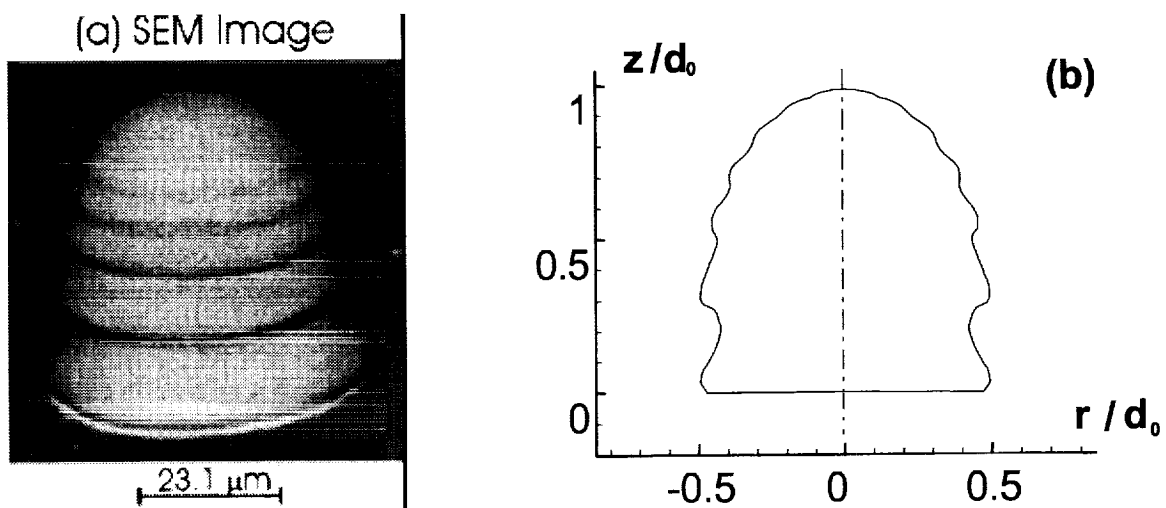
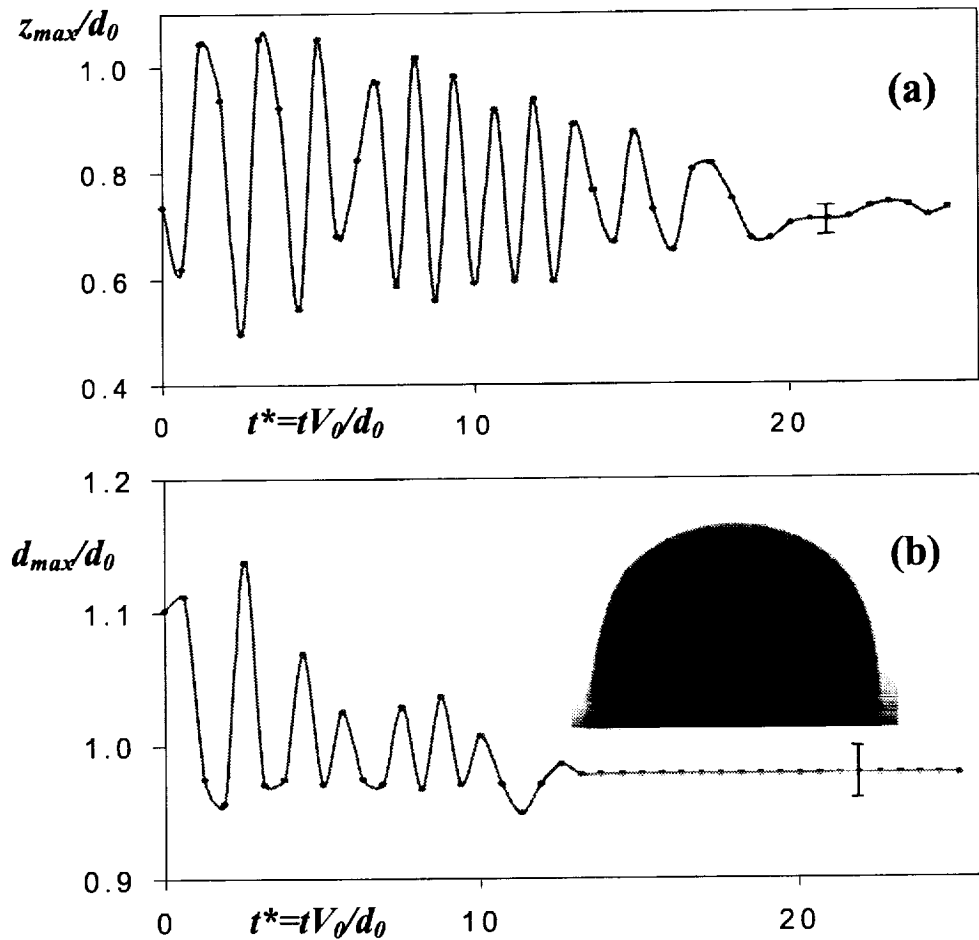
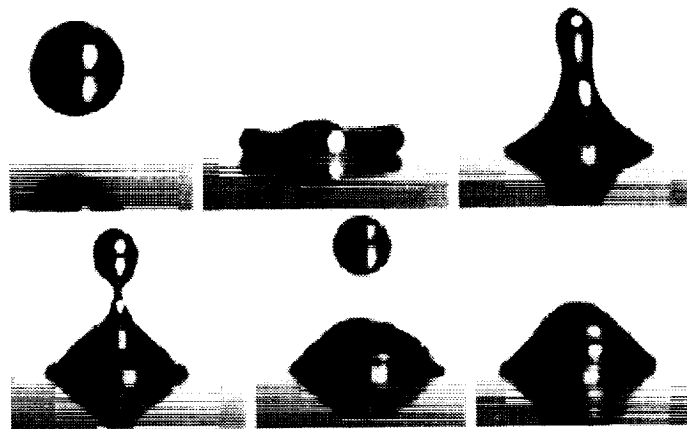


Fig. 3 (a) Solder bump geometry obtained in the microdroplet experiments for the baseline jetting conditions ( $Re=266$ ,  $We=3.23$  and  $Fr=4930$ ). (b) Model-predicted shape providing best agreement between experiment and modeling. In order to achieve this agreement, a phase-dependent value of  $Bi$  was used:  $Bi_l=0.5$  for liquid solder/substrate contact,  $Bi_s=0.0275$  for solid solder/substrate contact.



**Fig. 4** Temporal variation of (a) dimensionless maximum droplet height  $z_{max}/d_0$ , and (b) maximum splat diameter  $d_{max}/d_0$  from impact up to complete solidification of a mm-sized solder droplet impacting on a stainless steel substrate ( $Re=1676$ ,  $We=7.4$  and  $Fr=37$ ). The error bars indicate the uncertainty due to pixel size resolution. The shape of the solidified bump is shown in the inset of frame (b).



**Fig. 5** Selected experimental images obtained using high-speed video when a 0.9mm solder droplet impacted on a smooth copper substrate ( $Re = 3200$ ,  $We = 27.7$  and  $Fr = 147.5$ ). Time proceeds from left to right and from top to bottom. Under these conditions, breakup of the droplet was observed at the end of the first recoiling cycle after impact.